AIP | Review of Scientific Instruments

Performance evaluation of a lossy transmission lines based diode detector at cryogenic temperature

E. Villa, B. Aja, L. de la Fuente, and E. Artal

Citation: Review of Scientific Instruments **87**, 014706 (2016); doi: 10.1063/1.4939730
View online: http://dx.doi.org/10.1063/1.4939730
View Table of Contents: http://scitation.aip.org/content/aip/journal/rsi/87/1?ver=pdfcov
Published by the AIP Publishing

Performance evaluation of a lossy transmission lines based diode detector at cryogenic temperature

E. Villa,[a] B. Aja, L. de la Fuente, and E. Artal
Departamento Ingeniería de Comunicaciones, Universidad de Cantabria, Plaza de la Ciencia s/n, 39005 Santander, Spain

(Received 1 October 2015; accepted 28 December 2015; published online 12 January 2016)

This work is focused on the design, fabrication, and performance analysis of a square-law Schottky diode detector based on lossy transmission lines working under cryogenic temperature (15 K). The design analysis of a microwave detector, based on a planar gallium-arsenide low effective Schottky barrier height diode, is reported, which is aimed for achieving large input return loss as well as flat sensitivity versus frequency. The designed circuit demonstrates good sensitivity, as well as a good return loss in a wide bandwidth at Ka-band, at both room (300 K) and cryogenic (15 K) temperatures. A good sensitivity of 1000 mV/mW and input return loss better than 12 dB have been achieved when it works as a zero-bias Schottky diode detector at room temperature, increasing the sensitivity up to a minimum of 2200 mV/mW, with the need of a DC bias current, at cryogenic temperature. © *2016 AIP Publishing LLC.* [http://dx.doi.org/10.1063/1.4939730]

I. INTRODUCTION

The use of Schottky diodes in wideband receivers has been demonstrated in several applications, such as spectroscopy, imaging, radio astronomy, or remote sensing.[1–4] These receivers are usually composed of diode mixers in millimeter and submillimeter wavelength, which are cooled down to cryogenic temperatures in order to have low noise and therefore to improve the sensitivity.[5–7] On the other hand, other types of microwave broadband receivers used in radio astronomy, as well as in other radio physics applications, usually have square-law detectors at their outputs, which make nonlinear transforms with the aim of obtaining an output DC value proportional to the variance of input noise-like signal.[8,9] These receivers are very sensitive radiometers, where the received microwave fluctuation electromagnetic radiation is detected with a Schottky diode working as square-law device.[10–13] In order to improve their sensitivity, these receivers are partially or fully cooled to cryogenic temperatures, and when a great level of integration in the system is required, such as in arrays of receivers, the diode detectors can be also working under cryogenic conditions.[14] The Schottky diode detectors are configured under different topologies,[15–20] but normally with reactive matching networks to compensate the impedance of the diodes over a wide frequency range.[15–17] Since the diode intrinsic sensitivity varies with frequency, good input matching and constant sensitivity over a wide frequency range are not achievable only with reactive matching networks. In this sense, the sensitivity flatness and the input return loss of the device are significant issues in this kind of receivers since the effective bandwidth is directly affected by the ripple in the responses.[21] Furthermore, the need of having a good input matching is required over the working bandwidth since the mismatching caused by each circuit or device that composed the system is directly observed in the full receiver response with high ripple.[21] Besides, the lack of a flat sensitivity significantly affects the effective bandwidth of the receiver.

This paper presents the analysis, design, and characterization of a square-law detector at room (300 K) and cryogenic (15 K) temperatures working in the Ka-band suitable for radio astronomy applications. The initial proposal for the detector is to be used at room temperature in the receiver of the QUIJOTE project[4] as part of the back-end module, but the operation at cryogenic temperature of the whole receiver is being considered in order to achieve a higher integration level, which is a significant issue when many pixels compose the full receiver.[14] In this case, it would be necessary to analyze and to model the performance of the diode and the detector with temperature. This work shows the analysis of a Schottky diode detector which is able to work at both room and cryogenic temperatures, considering the behavior of the diode over the temperature. Besides, the comparison between both physical temperature performances of the diode and the detector is described, modelling and analyzing their behaviors.

The document is divided into four sections. The first one gives an introduction and, then, the modelling of DC and radio frequency performances of a Schottky diode at room and cryogenic temperature and the design of the detector circuit are analyzed and described in Section II. The experimental results at both physical temperatures are presented and discussed in Section III. Finally, Section IV draws general conclusions.

II. DETECTOR DESIGN

A. Design discussion

Most of the detector designs reported in the literature are developed without the need of having a flat sensitivity response over a frequency range.[15–20] In this case, although the intrinsic sensitivity of the diode is not flat with the frequency, the input

[a]Author to whom correspondence should be addressed. Electronic mail: villae@unican.es

network does not need to compensate it, and only the matching issue is concerned.

Moreover, significant return loss is required in order to have a low ripple response receiver, which improves its effective bandwidth.

Considering the matching network needed to be added to the diode, when reactive matching based on microstrip transmission lines technology is used,[15,19,20] a non-flat sensitivity is achieved within the bandwidth. On the other hand, a resistive match using a shunt resistor[15] can provide a good broadband return loss but at the expense of voltage conversion ratio.

Therefore, the solution implemented in this work employs a matching network which introduces additional losses to the circuit, but it allows the compensation of the intrinsic sensitivity curve of the diode. Besides, the lossy microstrip lines network enable to achieve good matching results within the desired frequency range.

B. Detector design development

The detector design is based on hybrid integration technology using a zero-bias gallium arsenide (GaAs) Schottky diode. Among the main specifications in the detector design are the input matching and the voltage sensitivity. During the design, two demanding requirements related to the sensitivity are taken into account: the magnitude of the sensitivity and its flatness response, both versus a wide frequency range.

The detector design is divided into different steps: first of all, it is needed to know the behavior of the Schottky diode over small-signal and large signal regimes; then, the design of a matching network intended to provide flat responses over a frequency range in terms of radio frequency input power to DC output voltage conversion and, additionally, a good behavior over a wide range of temperatures. Therefore, the analysis of a suitable matching network must include as load the variation of the Schottky diode impedance over the analyzed frequency range, in order to get an equalized response over the whole band. Hence, a model for the Schottky diode is developed and used for the analysis.

1. Schottky diode model extraction

The chosen diode is a GaAs planar-doped low-barrier Schottky type. This is a zero-bias beam-lead diode model HSCH-9161 from Agilent Technologies with a cut-off frequency above 110 GHz, which makes it suitable to be used at microwave frequencies.

Facing the possibility of having the same diode detector design working under both room and cryogenic temperatures, measurements of the Schottky diode were made in order to obtain an accurate model which predicts its behavior. The operation of a radio astronomy receiver at cryogenic temperature is focused on the minimum reachable temperature, so the model extraction and performance test presented in this document are fulfilled only at two physical temperatures: room temperatures of 300 K and 15 K as the cryogenic one. Since there is not a small-signal model for the diode working under cryogenics, a new one is developed for both physical temperatures in order to improve its accuracy, to provide further data about the diode (saturation current or ideality factor), and to foresee the cryogenic behavior which is not provided by the manufacturer, as well as the non-linear response in the large signal regime.

The model of the diode comprises of DC, radio frequency, and non-linear performances through the measurement of the current-voltage (I-V) feature and the small signal scattering parameters up to 40 GHz at room (300 K) and cryogenic (15 K) temperatures.

In order to properly model the diode, the basic parameters of a Schottky junction, such as the saturation current I_S, the ideality factor n, and the equivalent series resistance R_S, are obtained based on the I-V curve.

By cooling the device, the threshold voltage shifts toward higher values due to an increase of the Schottky barrier height.[22,23] Under no bias condition, the higher barrier voltage implies a higher dynamic resistance, which is defined as the change in current in the diode caused by a small change in voltage across the diode at a fixed bias point. The increment in the resistance prevents from delivering enough signal into the diode in order to provide a detected voltage. This is solved applying an additional DC bias current to bias the diode in a region of its characteristic curve with appropriate dynamic resistance.[23] Additionally, the ideality factor in the model of the Schottky diode is temperature-sensitive, increasing its value as the temperature decreases.[22] Hence, the model obtained considers the zero-bias condition of the diode at room temperature, while a bias-dependence feature, when cryogenic temperature is applied.

The model is performed in different steps. Initially, the I-V feature is fitted, according to the exponential I-V expression of a diode current given by

$$I = I_S \cdot \left(e^{\left(\frac{q \cdot (V_C - I \cdot R_S)}{n \cdot k \cdot T} \right)} - 1 \right), \tag{1}$$

where I_S is the saturation current (A), V_C is the applied voltage to the diode (V), n the ideality factor, R_S is the equivalent series resistance of the diode (Ω), k the Boltzmann constant, q the electron charge, and T the physical absolute temperature (K).

The equivalent series resistance R_S is modelled using a pair of shunt individual resistances (R_{S1} and R_{S2}) in order to accomplish the dual behavior at room and cryogenic temperatures. Both resistances R_{S1} and R_{S2} are defined to provide the zero-bias, forward, and reverse conditions of the diode at both temperatures. The resistance R_{S1} has a dependence on the voltage and current of the diode,[24] given by

$$R_{S1} = \frac{0.001 \cdot V_{\min}}{I + 10^{-30}} - \frac{1}{I + 10^{-30}} \cdot \left[(V_C - V_{\min}) - \frac{n \cdot k \cdot T}{q} \cdot \left(\ln\left(I + 10^{-30}\right) - \ln\left(I_{\min}\right) \right) \right], \tag{2}$$

where the values of V_{min} and I_{min} are defined by a point in the linear region of the I-V curve (listed in Table I) and V_C is the applied voltage to the diode (V). When working at room temperature, this resistance takes an infinite value so its effect is negligible.

TABLE I. Schottky diode HSCH-9161: saturation current (I_S), ideality factor (n), and constant resistance (R_{SC}).

Parameter	Room temperature (300 K)	Cryogenic temperature (15 K)
n — ideality factor	1.32	6.21
I_S — saturation current (A)	6.33×10^{-6}	2.34×10^{-19}
R_{SC} — constant resistance (Ω)	43.2	20
V_{min} (V)	0.06	0.205
I_{min} (A)	3.53×10^{-5}	3.07×10^{-8}

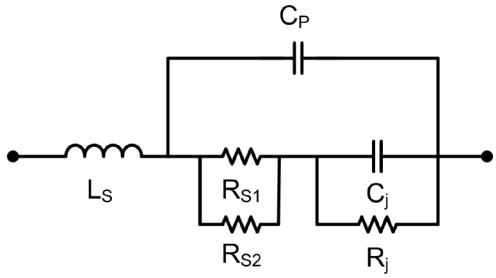

FIG. 1. Small signal model of the diode HSCH-9161.

Besides, the resistance R_{S2} shows a dependence with the current of the diode, given by

$$R_{S2} = R_{SC} \cdot \left(1 + 10^6 \cdot I\right), \tag{3}$$

where R_{SC} is a constant value obtained from the non-linear region of the I-V feature of the diode.

Then, the small signal model is fitted using the parameters (n, I_S, and R_{SC}) obtained in the I-V fitting and the measured scattering parameters. The small signal model of the diode is shown in Fig. 1. The model of the Schottky junction is performed with a shunt circuit composed of a capacitance C_j, which models the junction capacitance, and a resistance R_j, which models the junction resistance and it is given by

$$R_j = \frac{n \cdot k \cdot T}{q} \cdot \frac{1}{I + I_s}, \tag{4}$$

where I is the current in the diode (A), I_S is the saturation current (A), n the ideality factor, k the Boltzmann constant, q the electron charge, and T the physical absolute temperature (K). Besides, parasitic elements (L_S and C_P) of contacts of the device are included.

The measurements of the DC and radio frequency responses are performed at both room and cryogenic temperatures in a coplanar probe station. The cryogenic test reached a temperature of 15 K. The measurements are done using a coplanar-to-microstrip transition to the anode of the diode and its cathode is connected to ground.

The DC features are tested using a semiconductor device parameter analyzer model B1500A from Agilent Technologies and a semiconductor parameter analyzer model 4155A from Agilent Technologies for cryogenic tests.

The I-V characteristics of the diode measured at both physical temperatures, and compared to the extracted model, are shown in Fig. 2. The parameters of the exponential expression of a diode current feature for both temperatures are listed in Table I. The model simulations are compared to measurements of several diodes, achieving good agreement in all of them.

The scattering parameters are tested using a network analyzer E8364A from Agilent Technologies, with an input power of −30 dBm in the frequency range from 1 to 40 GHz. A low input power level is used since noise-like signals with a low signal power will be measured when working in the radiometer. The measurement at room temperature is performed under zero-bias condition, while at cryogenic temperature the parameters are tested for different diode currents. The measurements at both temperatures are performed in a cryogenic probe station using a LRM (Line-Reflect-Match) standards calibration technique. Fig. 3 shows the diode impedance from 1 to 40 GHz, at room temperature (zero-bias) and at cryogenic temperature from zero bias up to 215 μA diode bias current. The input matching depends on the diode junction resistance (R_j) which at the same time depends on the temperature and the DC bias for small signal operation.[25] The small signal model of the diode used in the simulation and depicted in Fig. 1 is fitted with the parasitic elements and the junction capacitance listed in Table II, which are considered constant with the temperature.

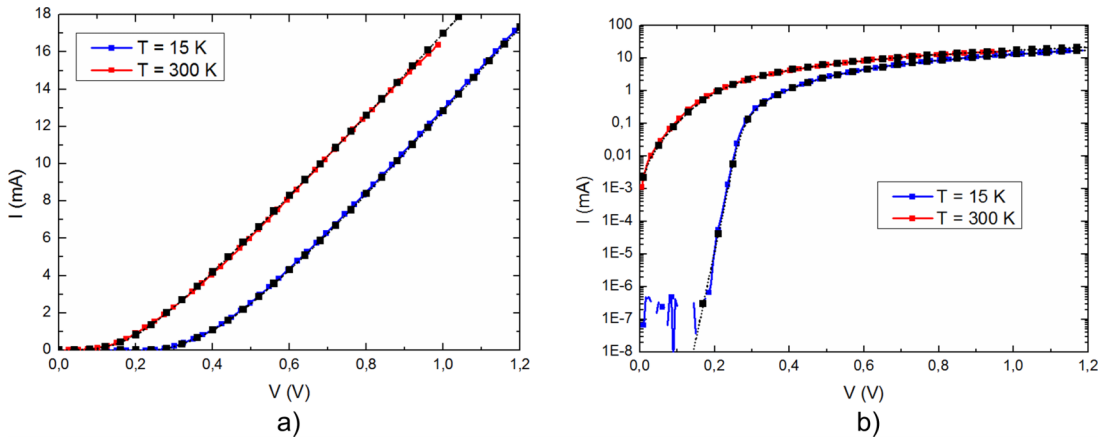

FIG. 2. I-V characteristic in black lines using the diode model (black squares), compared to room temperature (300 K) measurements (red) and cryogenic temperature (15 K) measurements (blue). (a) Linear scale. (b) Logarithmic scale.

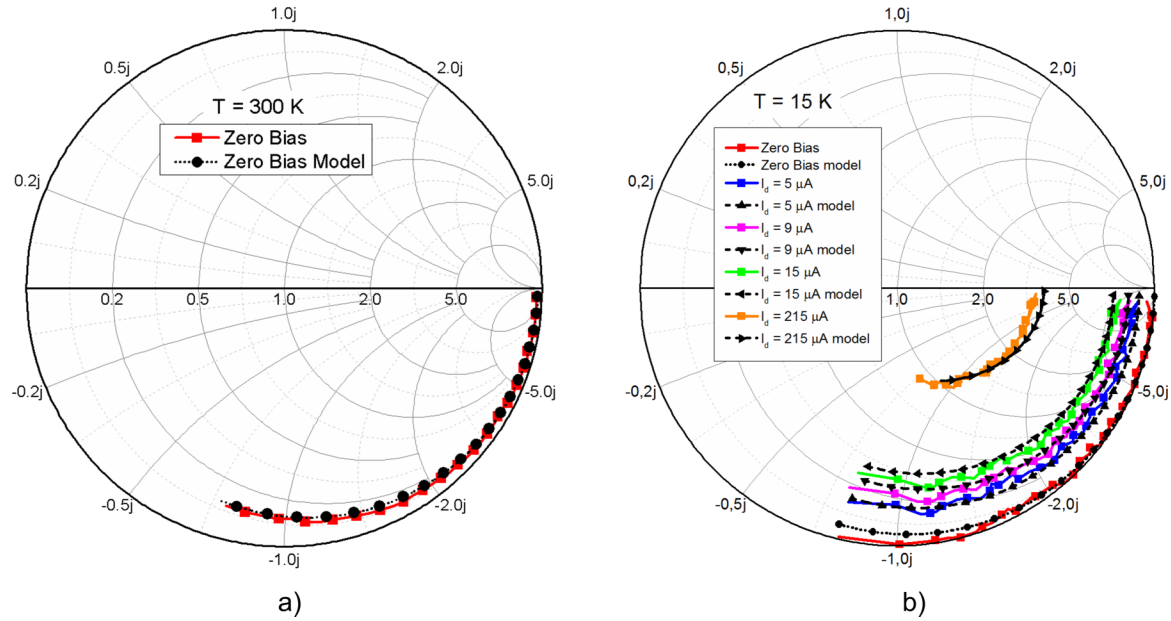

FIG. 3. Input impedance of the diode HSCH-9161 (1–40 GHz). (a) At room temperature (300 K) under zero-bias. (b) At 15 K for different diode bias currents.

Finally, a non-linear model of the diode is made in order to verify its radio frequency-to-DC response working as a detector diode. The non-linear model employs an electrical circuit of a diode junction[26] using the features obtained from the DC and small signal modelling. The model is temperature dependent and its currents and conductances are calculated from the input parameters $(I_S, n, C_j, \ldots)$.

As this diode is going to be used in a microwave detector, the voltage sensitivity parameter S_{DIODE} is defined as the conversion ratio between the DC voltage, V_{DC} (V), at the output of the device and the available power, P_{avs} (W), of an input radio frequency signal to the device, given by

$$S_{DIODE} = \frac{V_{DC}}{P_{avs}}. \tag{5}$$

Using the parameters obtained from the fitting of the I-V characteristic and the small signal scattering parameters at room temperature, the sensitivity predicted by the non-linear model is simulated. This result is shown in Fig. 4 for a fixed frequency of 31 GHz versus available power, together with the measurement of the conversion of the diode under zero-bias. Both the prediction of the model and the measurement are performed with the cathode of the diode connected to a high impedance load. The sensitivity of the diode shows compression for available powers above −27 dBm. These results show a good agreement between measurement and simulation using the model at room temperature, so it validates its use as design tool under zero-bias conditions at 300 K. The difference between the measured and simulated sensitivity is due to the slight deviation in the input reflection coefficient between the model and the measurement, which is lower than 0.1 dB in the whole frequency band.

TABLE II. Small signal model parameters of the Schottky diode HSCH-9161: parasitic inductance and capacitance (L_S, C_P) and zero-bias junction capacitance (C_j).

Parameter	Value
L_S	155 pH
C_P	0.035 pF
C_j	0.018 pF

2. Matching network design

The basic schematic considered for the detector is shown in Fig. 5.

From the diode model, the HSCH-9161 is not a good match to 50 Ω because of the high value of the junction resistance R_j and other parasitic effects. So it is needed to synthesize an input matching network that would transform its impedance in the frequency band of interest (20% of bandwidth at 31 GHz). The input matching should work for the whole bandwidth, 26 GHz–36 GHz, and for the range of

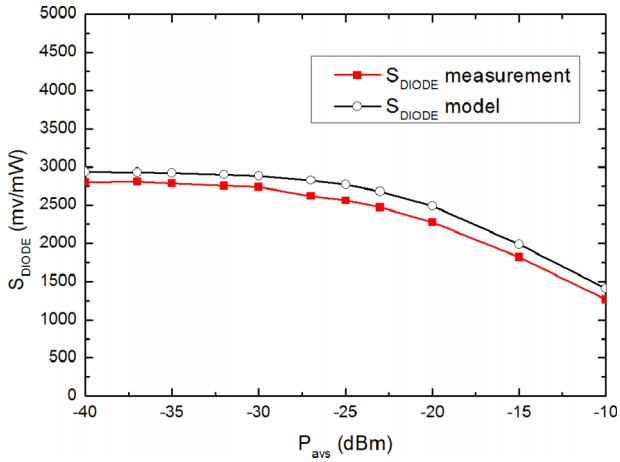

FIG. 4. Sensitivity measured and simulated of the diode HSCH-9161 at room temperature under zero-bias for a power sweep of the input signal at a frequency of 31 GHz.

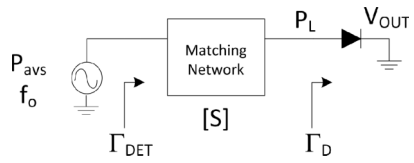

FIG. 5. Basic detector schematic including the matching network.

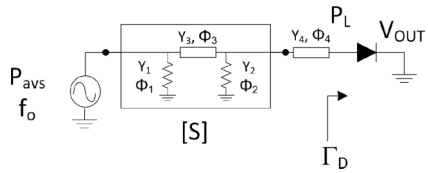

FIG. 6. Detector schematic including the lossy transmission line matching network.

input power levels in a radio astronomy application, which are expected to be low. Therefore, the matching network desired would match the diode in order to achieve input return loss better than 10 dB within the band in the detector.

Considering the schematic shown in Fig. 5, the input reflection coefficient of the detector can be approached as

$$\Gamma_{DET} = S_{11} + \frac{S_{21} \cdot S_{12} \cdot \Gamma_D}{1 - \Gamma_D \cdot S_{22}}, \tag{6}$$

where the S_{11}, S_{21}, S_{12}, and S_{22} are the corresponding scattering parameters of the matching network and Γ_D is the input reflection coefficient of the small signal model of the diode, while the sensitivity of the detector is given by

$$S_{DET} = G_T \cdot \frac{S_{DIODE}}{1 - |\Gamma_D|^2}, \tag{7}$$

where S_{DIODE} is the sensitivity of the non-linear model of the diode and G_T is the transducer gain of the matching network given by

$$G_T = \frac{P_L}{P_{avs}} = |S_{21}|^2 \cdot \frac{1 - |\Gamma_D|^2}{|1 - \Gamma_D \cdot S_{22}|^2}, \tag{8}$$

where P_{avs} is the available power at the input of the detector and P_L is the power delivered to the diode.

In the detector design, the matching network is focused on providing the available power to the diode from 26 to 36 GHz with large return loss and, simultaneously, a flat sensitivity in this frequency range.

When a lossless matching network is considered, reciprocal behavior and unitary matrix are expected for the network. In case of perfect match, the transducer gain of the matching network has unity value since the delivery power is equal to the available power. Then, a desirable large return loss is obtained but the sensitivity of the detector is the same as the sensitivity of the diode, whose performance is not flat versus the frequency. On the other hand, if a poor input return loss level in wideband operation is considered using lossless matching network, a flat sensitivity in the bandwidth could be achieved, but the input matching result makes it unsuitable. Both scenarios would return in a reduction of the effective bandwidth due to the lack of flatness or the increase in the ripple of the expected response and, therefore, a lower sensitivity of the receiver.[21]

Hence, a lossy matching network has been considered in order to compensate the slope in the sensitivity of the diode as well as to achieve large return loss in the detector. The proposed matching network is designed combining microstrip low-loss and lossy transmission lines.[27] The lossy transmission lines, implemented with thin-film resistors, are performed using distributed elements directly etched over the substrate, which avoid the use of interconnection elements if lumped resistors were used, and additionally their performance is stable with the temperature.[28] The network is configured in a π-topology in which the shunt transmission lines are lossy lines emulating distributed resistors and the equivalent circuit of the detector is shown in Fig. 6.

The equivalent admittance matrix of a short-circuited π-network such as the one depicted in Fig. 6 is given by

$$[Y]_{LOSSY} = \begin{bmatrix} Y_1 \cdot \coth(\Phi_1) - j \cdot Y_3 \cdot \cot(\Phi_3) & -j \cdot Y_3 \cdot \csc(\Phi_3) \\ -j \cdot Y_3 \cdot \csc(\Phi_3) & Y_2 \cdot \coth(\Phi_2) - j \cdot Y_3 \cdot \cot(\Phi_3) \end{bmatrix}, \tag{9}$$

where $Y_1 = 1/Z_1$, $Y_2 = 1/Z_2$, and $Y_3 = 1/Z_3$ are the admittances of the input shunt, output shunt, and series transmission lines of the π-network and Φ_i their electrical lengths, respectively.

3. Detector circuit

A complete analysis of cascaded matrixes is performed as the combination of the matrix of the matching network defined in Eq. (9) and the additional transmission line with electrical length Φ_4. The analysis enables the calculation of the widths and physical lengths of the lossy transmission lines considering a 20 Ω per square of sheet resistance in the frequency band from 26 to 36 GHz, while the series lossless transmission lines are set to a fixed impedance and electrical length values Z = 50 Ω, in order to avoid discontinuities in the microstrip lines.

The design of the input matching network using short-circuited lossy microstrip lines, via holes to ground, as thin film resistors (TFRs), provides a DC current return path to ground for the diode. Therefore, the output network of the detector does not need to have a physical ground return, which

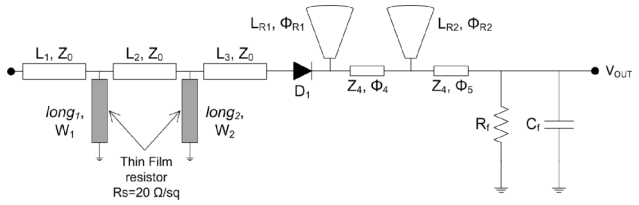

FIG. 7. Square-law detector schematic.

enables the use of this point as a possible DC bias point. The full schematic of the detector is shown in Fig. 7.

The radio frequency short-circuit is approached using a radial stub at the cathode of the diode, which forms a radio frequency ground providing what is known as the video capacitance of the detector. The use of this type of virtual ground enables the measurement of the DC voltage. The virtual ground is composed of two radial stubs in order to assure a good radio frequency ground in the whole band of interest, and between them a high impedance quarter-wavelength (Z_4, Φ_4) microstrip line is used. Both radial stubs are tuned in slightly different frequencies to assure their effect in different subbands. An extra high impedance (Z_4, Φ_5) microstrip line is placed at the output of the second radial stub to connect a low-pass filter, which is added at the output of the network in order to determine the upper frequency limit of the video bandwidth. The low-pass filter is implemented with surface mount devices (SMD), which have a stable dielectric material with the temperature, in order to ensure their performance at cryogenic temperature. The SMD capacitors are made of NP0/C0G dielectric, which shows a negligible temperature coefficient. This means that under cryogenic temperature the value of the component is almost invariant from the nominal value at room temperature.

The optimization of the circuit is performed taken into account the radio frequency-to-DC conversion and the input return loss simultaneously, in order to obtain a sensitivity of around 1000 mV/mW and return loss better than 10 dB. Besides, the low-pass filter is configured with a resistor Rf = 100 kΩ and a capacitor Cf = 100 pF, which defines a cutoff frequency of around 16 kHz. The final dimensions obtained in the optimization process are listed in Table III, in which the lengths of the TFRs are not included.

The TFRs are divided into small sections in order to have a better solution in terms of the layout, since a long line makes difficult to perform a suitable layout with a feasible area. The equivalent lengths, joining the different sections, for $long_1$ and $long_2$ are, respectively, 520 μm and 1665 μm.

The detector is designed on an alumina substrate composed of a gold conductive layer with a 20 Ω per square

TABLE III. Physical dimensions of the detector.

Variable	Value	Variable	Value
Z_0	50 Ω	L_1	100 μm
Z_4	85 Ω	L_2	800 μm
$W_1 = W_2$	170 μm	L_3	1200 μm
Φ_{R1}	90°	L_{R1}	550 μm
Φ_{R2}	90°	L_{R2}	550 μm
Φ_4	93°	Φ_5	93°

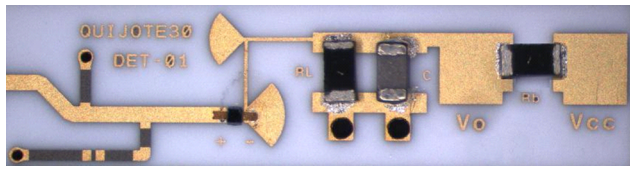

FIG. 8. Photograph of the square-law detector. Size: 10.5 mm × 2.7 mm.

nickel-chromium resistive layer of around 0.075 μm thickness underneath. The nickel-chromium layer shows a stable resistivity with the temperature.[28] The alumina substrate has εr = 9.9 with a 254-μm thickness and a loss factor of 0.0001. The beam lead diode, SMD components, and the substrate are glued to the substrate and the chassis, respectively, using a conductive silver epoxy H20E from Epo-tek. A photograph of the manufactured and assembled detector is shown in Fig. 8.

III. EXPERIMENTAL RESULTS

The characterization of the detector is performed at room temperature in the coplanar probe station, and at cryogenic temperature inside the cryostat. For the cryogenic test, the circuit is assembled in a chassis.

Initially, the measurement of the input return loss at room temperature in the coplanar probe station is performed. The measurement and the simulation results of the detector are shown in Fig. 9, including both a coplanar-to-microstrip transition. The result at cryogenic temperature is not very accurate since the measurement reference plane is not at the input of the detector, so the input return loss is severely masked by the access cable and feedthrough to the cryostat. Besides, cryogenic calibration techniques involve several thermal cycles so measurement drifts could be present and inaccurate results would be obtained.

The input reflection coefficient of the diode under cryogenic conditions for low currents is close to its zero-bias room temperature reflection coefficient. This similarity between the reflection coefficients at both temperatures can be seen comparing Fig. 3(a) with Fig. 3(b) for low bias points. Besides, the input matching network performance is stable with the temperature. Therefore, the input reflection coefficient

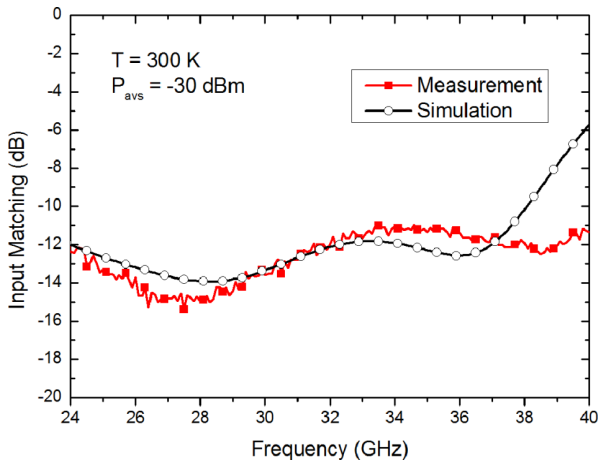

FIG. 9. Input matching of the detector at room temperature (300 K) in red line compared to simulation results in black line.

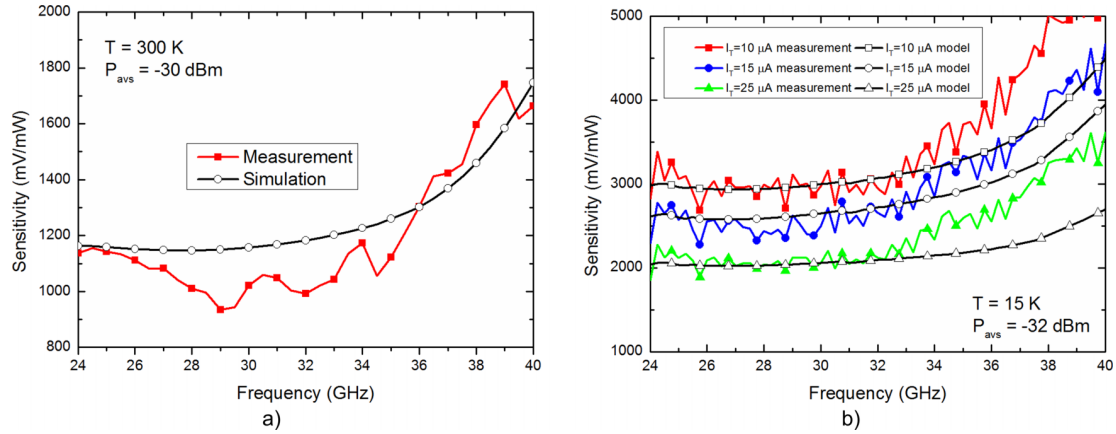

FIG. 10. Detector sensitivity versus frequency. (a) Measurement (red) zero-bias for a continuous wave input signal of −30 dBm compared to simulation (black) at room temperature 300 K. (b) Measurement (green, blue, and red) for a continuous wave input signal of −32 dBm with different diode bias currents compared to simulations (black) at 15 K ambient temperature.

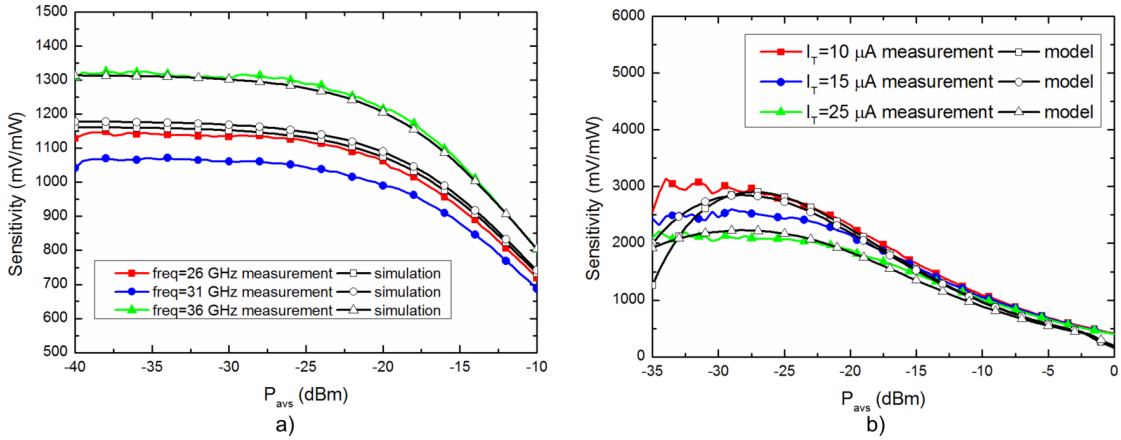

FIG. 11. Sensitivity versus input power for a continuous wave input signal of 26 GHz, 31 GHz, and 36 GHz. (a) Zero-bias at 300 K ambient temperature. (b) Different diode bias currents at 15 K ambient temperature for a continuous wave input signal of 31 GHz.

of the detector at cryogenic temperature, when a low current flows in the diode, is expected to be as good as the one at room temperature.

Afterwards, the sensitivity of the detector versus frequency for a fixed input power is measured at both physical temperatures (300 K and 15 K). The results are compared to the simulations of the detector, using the model of the diode at the specific temperature with the measured input power and applying the proper diode DC current at cryogenic temperature. The results are shown in Fig. 10(a) for room temperature under zero-bias condition and in Fig. 10(b) for several bias points at cryogenic temperature. The deviations in the sensitivity results are due to slight differences between the input reflection coefficient of the model and the measurement and the losses of the lossy matching network.

Additionally, a sweep of input power is performed for several frequencies within the band, in order to obtain the dynamic range of the detector. The sensitivity versus input power at three frequencies is shown in Fig. 11(a) at room temperature. The same sweep of the input power is performed at cryogenic temperature (15 K) considering a single continuous wave input signal of 31 GHz since several bias points are analyzed. The sensitivity at 15 K, applying to the diode currents between 5 μA and 25 μA, is shown in Fig. 11(b). From the results, the dynamic range of the detector increases for higher currents while the sensitivity decreases at cold temperatures.

TABLE IV. Mean values of the sensitivity (26–36 GHz) for an input power of −32 dBm and the input power for 1-dB compression point of the detector at 31 GHz working at 15 K for different current bias applied to the diode.

Bias conditions (μA)	S (mV/mW)	P_{1dB} (dBm)
$I_d = 10$	3144 ± 530	−21.5
$I_d = 15$	2715 ± 520	−21
$I_d = 25$	2217 ± 350	−19.5

To summarize the results at room temperature, a flat sensitivity is measured with a mean value of the sensitivity in the frequency band from 26 to 36 GHz of 1066 mV/mW ± 120 mV/mW for an input power of −30 dBm, return loss better than 12 dB and a 1-dB compression point of around −15 dBm input power is achieved. A maximum input power of about −23 dBm can be used in order to disregard compression effects in the detected voltages. On the other hand, the summary of the results at a cryogenic temperature of 15 K is listed in Table IV for the different applied currents to the diode, showing an increase in the sensitivity of the detector with respect to the room temperature measurement, which depends on the bias current of the diode. Moreover, the higher

TABLE V. Performance comparison.

References	Operation temperature (K)	Bandwidth (GHz)	Sensitivity (mV/mW)	Flat response	Input matching (dB)	Technology
15	300	3 @ L/S-band	350	No	...	Microstrip hybrid
16	300	Single frequency (89 GHz)	8600	No	<-10	Microstrip hybrid
17	300	17 (1-18 GHz)	1000	Yes	<-18	MMIC — antiparallel diodes
18	300	25 @ W-band	400-7700	No	<-1	Coplanar MMIC
19	300	40 @ V/W-band	2000-6000	No	<-2	Microstrip hybrid
This work	300	10 @ Ka-band	1000	Yes	<-12	Hybrid — lossy lines
	15		2200	Yes	...	

the bias point, the lower the sensitivity of the detector. Besides, the compression of the detector also depends on the applied bias point, and the higher the diode current, the better the compression level and the flatness of the sensitivity versus frequency.

Finally, Table V gives the performance comparison of the presented detector with other published designs. Although, several technologies are used in the designs, such as monolithic or hybrid technologies, the proposed design based on lossy transmission lines improves the flatness of sensitivity using a single Schottky diode with good return loss. On the other hand, this work provides a successful performance of the detector under cryogenic temperature.

IV. CONCLUSION

This work presents a squared law-detector design and fabrication and its performance analysis when its physical working temperature is modified from ambient temperature (300 K) to a cryogenic condition (15 K). The detector was designed using an extracted model of Schottky diode based on measurements at both temperatures. Besides an input matching network was designed considering the goals of large input return loss and flat sensitivity versus frequency, as well as stable behavior versus temperature. The detector has performed successfully at room temperature (300 K) with a flat sensitivity performance versus frequency of around 1000 mV/mW ± 120 mV/mW from 26 to 36 GHz. Furthermore, the detector also showed return loss better than 12 dB and input power for 1 dB compression of about −23 dBm at 300 K. On the other hand, the same detector working at cryogenic temperature (15 K) has exhibited a sensitivity of about 2200 mV/mW with flatness ± 350 mV/mW versus frequency and input power for 1 dB compression of about −19.5 dBm when a DC current of 25 μA is applied to the detector.

ACKNOWLEDGMENTS

This work has been funded by the Spanish Ministry for Economy and Competitiveness under the CONSOLIDER-INGENIO 2010 programme under the Reference No. CSD2010-00064. The authors would like to thank Eva Cuerno and Ana Pérez for the assistance in the assembly of the circuit.

[1]P. H. Seigel, IEEE Trans. Microwave Theory Tech. **50**, 910 (2002).
[2]B. H. Deng, C. W. Domier, N. C. Luhman, Jr. *et al.*, Rev. Sci. Instrum. **72**, 301 (2001).
[3]D. Woolard *et al.*, in Proceedings of 22nd Army Science Conference, 2000.
[4]E. Artal *et al.*, in *Proceedings of International Conference on Electromagnetics in Advanced Applications* (IEEE, 2013), p. 250.
[5]T. W. Crowe and R. J. Mattauch, in *Proceedings of IEEE MTT-S International Symposium Digest* (IEEE, 1987), p. 753.
[6]B. A. Rozanov and S. B. Rozanov, in *Proceedings of Physics and Engineering of Millimeter and Submillimeter Waves MSMW'98, 3rd International Kharkov Symposium* (IEEE, 1998), p. 104.
[7]O. P. Koistinen, H. T. Valmu, A. Raisanen, V. F. Vdovin, Y. A. Dryagin, and I. V. Lapkin, IEEE Trans. Microwave Theory Tech. **41**, 2232 (1993).
[8]J. D. Kraus, *Radio Astronomy*, 2nd ed. (Cygnus-Quasar Books, 1986).
[9]M. E. Tiuri, IEEE Trans. Antennas Propag. **12**, 930 (1964).
[10]N. W. Boggess, J. C. Mather, R. Weiss, C. L. Bennet, E. S. Cheng, E. Dwek, S. Gulkis, M. G. Hauser, M. A. Janssen, T. Kelsall, S. S. Meyer, S. H. Moseley, T. L. Murdock, R. A. Shafer, R. F. Silverberg, G. F. Smoot, D. T. Wilkinson, and E. L. Wright, Astrophys. J. **397**, 420 (1992).
[11]N. Jarosik, C. L. Bennett, M. Halpern, G. Hinshaw, A. Kogut, M. Limon, S. S. Meyer, L. Page, M. Pospieszalski, D. N. Spergel, G. S. Tucker, D. T. Wilkinson, E. Wollack, E. L. Wright, and Z. Zhang, Astrophys. J., Suppl. Ser. **145**, 413 (2003).
[12]E. Artal, B. Aja, M. L. de la Fuente, J. P. Pascual, A. Mediavilla, E. Martinez-Gonzalez, L. Pradell, P. de Paco, M. Bara, E. Blanco, E. García, R. Davis, D. Kettle, N. Roddis, A. Wilkinson, M. Bersanelli, A. Mennella, M. Tomasi, R. C. Butler, F. Cuttaia, N. Mandolesi, and L. Stringhetti, J. Instrum. **4**, T12003 (2009).
[13]E. Villa, J. L. Cano, J. Cagigas, D. Ortiz, F. J. Casas, A. R. Pérez, B. Aja, J. V. Terán, L. de la Fuente, E. Artal, R. Hoyland, and A. Mediavilla, Rev. Sci. Instrum. **86**, 024702 (2015).
[14]C. Bischoff *et al.*, Astrophys. J. **768**, 1 (2013).
[15]S. Qayyum, M. D. Wei, and R. Negra, in *Proceedings of 44th European Microwave Conference* (IEEE, 2014), p. 758.
[16]M. Hoefle, A. Penirschke, O. Cojocari, T. Decoopman, M. Tier, P. Piironen, M. G. Périchaud, and R. Jakoby, Electron. Lett. **50**, 606 (2014).
[17]A. S. Zagorodny, N. N. Voronin, I. V. Yunusov, and V. A. Gushchin, in *Proceedings of 15th International Conference on Micro/Nanotechnologies and Electron Devices EDM* (IEEE, 2014), p. 164.
[18]F. Thome, A. Leuther, S. Maroldt, M. Schlechtweg, and O. Ambacher, IEEE Microwave Wireless Compon. Lett. **24**, 860 (2014).
[19]M. Hrobak, M. Sterns, M. Schramm, W. Stein, and L. P. Schmidt, in *Proceedings of 43rd European Microwave Conference* (IEEE, 2013), p. 179.
[20]H. Ito, T. Yoshimatsu, H. Yamamoto, and T. Ishibashi, in *Proceedings of 38th International Conference on Infrared, Millimeter, and Terahertz Waves* (IEEE, 2013), p. 1.
[21]B. Aja, E. Artal, L. de la Fuente, and J. P. Pascual, in *Proceedings of 36th European Microwave Conference* (IEEE, 2006), p. 1501.
[22]S. M. Sze, *Semiconductor Devices: Physics and Technology* (Wiley, New York, 1985).
[23]D. M. Kim, D. H. Kim, and S. Y. Lee, Solid-State Electron. **51**, 865 (2007).
[24]V. L. Borblik, Y. M. Shwarts, and M. M. Shwarts, Semicond. Phys., Quantum Electron. Optoelectron. **12**, 339 (2009), see http://journal-spqeo.org.ua/n1_2009/n1_2009_contents.htm.
[25]I. Bahl and P. Bhartia, *Microwave Solid State Circuit Design* (Wiley, New York, 1988).
[26]P. Antognetti and G. Ambrosio, *Semiconductor Device Modeling with SPICE*, 2nd ed. (McGraw-Hill, 1993).
[27]B. C. Wadell, *Transmission Line Design Handbook* (Artech House, 1991).
[28]T. M. Flynn, *Cryogenic Engineering* (Marcel Dekker, 2005).